

An Innovative Hybrid Grid Integration Strategy for Solar PV, Wind, and Fuel Cells with Battery Storage, Empowered by Artificial Neural Networks

¹Talabathula Manga, Kasarapu Sathish Kumar²

¹M.Tech (PSA), EEE, Sanketika Vidya Parishad Engineering College., India

²Assistant Professor, EEE, Sanketika Vidya Parishad Engineering college., India

E-mail: manga762000@gmail.com, sathishkumar342@gmail.com

ABSTRACT:

The modelling, control, energy management, and operation of a hybrid grid-connected system with a fuel cell (FC), an electrolyser, and a photovoltaic (PV) battery energy storage system (BESS) are all covered by the proposed study. It has been suggested to create a hybrid PV-Wind-FC system with an electrolyser made of BESS and the fewest converters and control loops possible. By doing away with the PV converter, the suggested hybrid system offers an affordable way to include PV into a hybrid system. This includes designing controllers for grid-connected hybrid systems that have an FC with an electrolyser as a tertiary source, a BESS as a secondary source, and a distributed generator that is renewable (wind and photovoltaic). Additionally, in order to achieve sufficient phase margin and totally eliminate steady state error, the lead compensator and integrator are employed. It introduces phase shift ϕ_s at a cross gain frequency (ω_{cut}) and boosts the controller's stability. When connected to the grid, the Grid Side Controller (GSC) has the ability to handle the utility grid's frequency. PV power is optimised in the suggested arrangement and fed into the grid via GSC. The grid station's load sharing is supported by the Rotor Side Converter (RSC) and GSC. Furthermore, the effect of the intermittent nature of electricity produced by PV and wind is eliminated by the suggested BESS controller that coordinates with FC. Hydrogen is produced by the electrolyser using surplus electricity produced by renewable distributed generating. When adverse weather conditions prevent sufficient power generation, FC uses this hydrogen again. The purpose of the energy management has been to minimise the intermittent and fluctuating nature of wind and photovoltaic sources, meet the load profile, and prevent

BESS overcharging. Service continuity and consistent power supply are ensured by this approach.

The suggested hybrid system's efficiency in comparison to the traditional hybrid system documented in the literature is validated by the Simulink model findings. Using a MATLAB Simulink model, the suggested system and analysis have been modelled and presented. Finally, a comparison between the system's energy management and that of the conventional power system has been made.

I. INTRODUCTION

Life has become much easier and more uncomplicated with the rise in domestic appliances that perform basic activities. On the other hand, as more household appliances become electric, the demand for electricity is rising. The production of power is always rising to meet the demand for electric power. To meet demand, more renewable and non-renewable generation are added to the power network. The power flow architecture is made more complex in different ways by each type of conventional and non-conventional source. Governments are working to integrate renewable energy sources into the national grid in order to supply the whole demand for electricity, as environmental concerns have grown over the past few decades. The current design for clean and green energy generation incorporates renewable energy sources, such as PV, FC, ultra-capacitor, WT, geothermal, etc. [1], [2]. Due to their low installation costs and high power-to-cost ratio, solar and wind energy are the most widely used renewable energy sources. These sources are used globally in a variety of configurations because they don't require fuel, unlike fuel cell stacks and biogas, etc. [3], [4], and [5]. The current design for clean and green energy generation incorporates renewable energy sources, such as PV, FC, ultra-capacitor, WT, geothermal, etc. [1], [2]. Due to

their low installation costs and high power-to-cost ratio, solar and wind energy are the most widely used renewable energy sources. These sources are used globally in a variety of configurations because they don't require fuel, unlike fuel cell stacks and biogas, etc. [3], [4], and [5]. Some sophisticated control techniques to reduce transient oscillations transmitted to the stator from the rotor side owing to wind speed fluctuations have been published by Liu et al. [10] and Xu et al. [11]. Nian and Song [12] have presented a voltage conditioning architecture that smoothes the active and reactive power generation in a DFIG power generation architecture by producing smooth transitions and reducing the harmonics in the current and voltage. PV arrays are an extremely efficient and manageable kind of power generating, in contrast to wind power generation. Unlike wind turbines, there is no noise pollution, no air pollution, and no mechanical upkeep. With their multiple gigawatt power generating capability, very large photovoltaic farms have been established, offering dependable power generation to fulfil the increasing demand for electric power [13], [14]. Single-stage or two-stage topologies are the two major methods used to integrate PV array electricity into the grid. Comparing the single stage to the two-stage integration topologies, the single stage contains fewer converters and power switches, but the control architecture required to enable the operation is more complicated. Controlling the electricity injected into the grid is often accomplished through the use of the Voltage 23246 Source Inverter (VSI) scheme.

Hybrid topology power generating has drawn a lot of interest because of its cost-effective and environmentally beneficial features. Because they provide complimentary electricity, PV and wind turbine power grids exhibit greater stability and may be built in a variety of weather circumstances [15], [16], [17], and [18]. Observations show that the two aforementioned categories of sustainable sources have additional development options [19], [20], and [21]. In general, during the day, more electricity is produced by photovoltaic cells and less power is produced by wind turbines. However, the amount of PV produced at night is negligible and almost non-existent because the wind is moving faster at night than it does during the day, which results in a considerable increase in the power generated by wind turbines. The relevant element is also seen at

different times of year. Similar to how wind is less accessible in the summer, when solar power is greater, and how wind velocity is higher in the winter, when solar energy is less practical. This factor has encouraged many analysts to search for ways to integrate two energy sources. A few questions about the validity, stability, and power quality of the entire system are raised by this assimilation [22]. Electric Energy Storage Systems (EESSs) provide a viable solution with less power fluctuation, improved power quality, energy, and less imbalance due to their renewable energy sources [23], [24], and [25]. Reasonably priced EESSs may have provided a vital solution to address the irregularity and unpredictability of the generation of Renewable Energy Sources (RES) [26], [27], [28]. Generally speaking, EESS makes it possible to generate electricity reliably in situations where alternative power-generating options are unavailable, costs are high, or demand is high [23], [29], [30]. Two criteria are used to categorise various energy storage systems: shape and function. Functional criteria are used to categorise EESS into two groups: those with high power ratings, such as supercapacitors, Super-Conducting Magnetic Energy Storage (SMES), batteries, and flywheels [30], and those with low power ratings, such as bulk batteries, solar cells, FCs, and flow batteries [31], [32], and [33]. Electrical energy may be stored in a variety of ways depending on its type, such as chemical, thermal, mechanical, or power, and it can be converted back into power when needed. In hybrid grid systems, EESS is the best choice for ensuring sovereignty and enduring power variability. Thus, it is imperative that we implement the Hybrid Energy Storage System (HESS) [34], [35], [36]. Accordingly, the battery's cycles of charging and discharging have a big influence on how long these systems last [37], [38], and [39]. Therefore, to increase the security of the energy supply from PV and wind turbine systems, a third energy source is needed. The advantages should guide the selection of a third power system. There is a possibility to increase PV systems with wind turbines with just minor modifications, according to several research in this field. In order to combine the PV and wind turbine into a hybrid system, [4] has used a three-phase square waveform converter. Another three-input dc-dc boost converter is being offered in [40] in order to focus more on the DC loads of the hybrid system. However, it is not logical to expand the aforementioned converters in a

hybrid system. A system of wind and photovoltaic power that focuses on the DC voltage's gradual change and the DC capacitor bank's smaller size was created in [41]. The state of charge (SOC) of the BESS has been managed in the systems in [42] and [43] to lessen the output power fluctuation. New methods for analysing have been provided by references [44] and [45]. Numerous studies have been conducted to provide innovative control approaches for hybrid systems. In order to smooth the active and reactive output power of hybrid systems, [12] suggested a modified control algorithm that concentrated on the fifth and seventh grid voltage harmonics. A two-layer constant power management strategy for wind farms with DFIGs has been documented in [46]. The DFIG DC connection and Super-Capacitor (SC) energy storage system are connected in this study. For hybrid RES, new power generation and cost reduction strategies have been given in [47]. There is just one control loop in the battery bank's control structure, which is described in this paper. An incorporated energy share technique between the battery and SC that is designed was suggested by the study in [48]. The DC-DC buck-boost converter is used to connect the battery to the DC bus in the first topology, and it is eliminated in the second design. DC-DC converters have also been used to switch power between DC bus and SC. The study in [49] outlines a technique for integrating and coordinating the operation of solar generators (PV) with management of MPPT and battery storage to provide voltage and frequency support to an islanded microgrid. In this study, the battery energy storage system is controlled by the control loop approach. Furthermore, grid-tied (hybrid) systems now have PV/MPPT/battery with active power management and reactive power control included.

The control algorithms show effective correspondence between MPPT, the inverter's control, and the charging and discharging of energy storage. Therefore, the aforementioned investigations primarily concentrated on the control design and power energy sources coordination, ignoring the suggested structure's efficiency and optimality. Additionally, the efficiency of the hybrid energy system has not been optimised. The PV converter has been left out of the potential design of a system with DFIG and PV, which has been presented by [19]. It should be mentioned that the rating of the PV converter and its capacity should match. The authors of this study showed that PV capacity may be much higher

than the grid side controller (GSC) rating. Following the consolidation of the PV and GSC converters, the new converter is used more frequently. One way to implement MPPT in [19] is to manage the DC link voltage. Nonetheless, there was significant power output variation with this design, and the DC link voltage saw significant oscillations under typical circumstances. Owing to the intermittent nature of PV and wind, the system's power requirements can be reduced in response to variations in wind speed and solar irradiation.

Nevertheless, the greatest amount of solar energy cannot be extracted with this design. Furthermore, GSC's potential is not being fully utilised.

To meet the short coming of [19] and [50] introduced BESS to the PV DFIG hybrid system with a dented control scheme. The oscillations in DC link voltage and GSC power have been stabilized up to a large extent. In this proposed configuration utilization of GSC has been improved and DC bus capacitor size has decreased. However, charging of the Battery and the discharging of BESS decreases the life span of batteries. Moreover, BESS alone cannot cater to the load demand when Wind and PV supply less power to DC links due to weather conditions. The battery's lifetime is shortened in this procedure by repeated charging and draining. Consequently, in order to support the supply to the grid-connected system and load, an additional energy source is required.

This study presents the addition of FC and Electrolyser as a third energy source to the PV-DFIG and BESS hybrid grid-connected system. It has been suggested to use a hybrid PV-Wind-BESS with FC and an electronic controller that requires the fewest control loops and converters. The suggested hybrid system does away with the PV converter, offering a financially sensible way to include PV into a hybrid system. This covers the design of controllers for grid-connected hybrid systems that have an FC with an electrolyser as a tertiary source, a BESS as a secondary source, and a renewable distributed generator (wind and PV) as the primary source. The following are the primary goals of the research and benefits of the suggested system:

- To create a PV DFIG-BESS configuration that is both economical and efficient, with fewer control loops utilising FC and Electrolyser.
- Common AC and DC bus voltage as well as MPPT are performed by the GSC controller.

- To reduce GSC power and DC link voltage fluctuation as much as possible.
- A new architecture for hybrid wind, photovoltaic, battery energy system, smart grid, and fuel cell that combines an electrolyser to achieve optimum and efficient control over the various sources, improving the quality of power supplied to the AC grid by controlling the voltage and frequency of the grid and guaranteeing service continuity.
- Putting in place and integrating the FC and electrolyser to increase the system's sustainability in situations when wind and solar PV electricity are dependent on the weather and when solar power is nil at night. As a result, BESS cannot provide the load demand on its own under long-term scenarios with no wind and solar PV or low wind and solar circumstances.
- To ensure steady functioning of the DC side while providing frequency assistance to the AC side.
- To show how well the suggested configuration works with MATLAB Simulink.

The remainder of the paper is arranged as follows: Section II provides an explanation of the proposed hybrid grid-connected system. System modelling and control are illustrated in Section III. Section IV covers energy management. The findings and system simulation are shown in Section V. Section VI has the conclusion.

II. PROPOSED HYBRID GRID CONNECTED SYSTEM DETAILS

Fig. 1 depicts the suggested system's configuration.

The suggested system's GSC and its control scheme are designed to keep the DC-bus voltage within the specified safe bounds by limiting it. The DC-link's voltage also enables the system to track the PV system's MPP. A BESS is connected to the system in order to safeguard the GSC against overloads. Using a DC/DC Buck Boost bidirectional converter, the BESS is linked to the DC bus and utilised as a storage device. PV electricity is zero at night, whereas wind and solar power are dependent on the weather. As a result, when there is little to no wind and PV energy, the battery cannot supply the entire load requirement.

Therefore, FC with an electrolyser is combined with the system in order to increase its sustainability. When PV and wind energy provide high power and the battery reaches its charge storage threshold, the electrolyser activates and stores excess energy. Hydrogen produced by the electrolyser may be stored and utilised as an input by FC. When there is insufficient power generation at the DC connection because of bad weather, FC uses hydrogen to create power.

III. CONTROL AND SYSTEM MODELLING

A. MODEL DEVELOPMENT FOR SOLAR PV

A photovoltaic array is made up of several solar cells that produce charge carriers in response to photons striking the array. If the photon's energy exceeds the semiconductor's band gap, the electrons are expelled and the current becomes low. In addition to the standard mono-crystalline solar cells, a variety of poly-crystalline solar cells are reasonably priced. Much study has been conducted up to this point in an attempt to determine an accurate solar equation that could be correlated with actual behaviour. Therefore, the PV arrays' cell properties are not up to par. A current source and a diode connected in parallel make up the ideal PV array architecture.

A photovoltaic array is made up of several solar cells that produce charge carriers in response to photons striking the array. If the photon's energy exceeds the semiconductor's band gap, the electrons are expelled and the current becomes low. In addition to the standard mono-crystalline solar cells, a variety of poly-crystalline solar cells are reasonably priced. Much study has been conducted up to this point in an attempt to determine an accurate solar equation that could be correlated with actual behaviour. Therefore, the PV arrays' cell properties are not up to par. A current source and a diode connected in parallel make up the ideal PV array architecture.

The single solar cell circuit shown in Fig. 2 consists of a current source, a Shockley diode, and parallel and series resistances, R_{per} and R_{ser} . The total current of the solar cell is the sum of the diode current and current source [51].

Equation (1) illustrates the mathematical expression for a single solar cell.

$$I = I_{PV} - I_o \left[e^{\frac{qv}{akT}} - 1 \right] \quad (1)$$

where I stand for the current of a single solar cell, IPV for the total current created by solar radiation, Io for reverse leakage current (saturation), T for the temperature of the diode (in Kelvin), q for electron charge, and k for the Boltzmann constant. Equation (1) does not provide all of the solar cell's characteristics. Because it incorporates both parallel and series resistances, this model is the most appropriate one for the given empirical conditions. The resistance between the solar cell and the terminal connection is referred to as Rser.

$$I = I_{PV} - I_o \left[e^{\frac{V+R_{ser}I}{V_{ia}}} - 1 \right] - \left(\frac{V+R_{ser}I}{R_{per}} \right) \quad (2)$$

where Vt is the thermal voltage and may be further computed using the calculation $V_t = kT/q$, where V is the combined terminal voltage of the solar cells. where Rser is the total series resistance, Rper is the total parallel resistance, and Vt is the thermal voltage. Resistance resulting from leaking current at the p-n junction is called Rper. Equation (2) can be altered based on the parallel and series arrangements of the solar cells in a PV array. An increase in the number of parallel cells raises a PV array's current level as well. In a similar vein, a PV array's voltage increases as the number of series cells does. As seen in equation (3), the charges generated by temperature and solar radiation are Ipv.

$$I_{pv} = (I_{pvn} - K_i \Delta T) \frac{G}{G_n} \quad (3)$$

Since the solar cell's parallel resistance is larger than its series resistance, the short current is roughly equal to the PV threshold current. Threshold PV current (Ipnv), current coefficient (Ki), and temperature difference (T) between nominal and real K: $T_n - T$, where Gn represents nominal solar radiation and Gisincident solar radiation. Gn and G are measured in W/m². Numerous studies have been conducted in this field, and numerous formulae for

the characteristics of solar cells and their designs have been created. The Ion is provided here as eq. (4).

$$I_{on} = \frac{I_{sen} + K_i \Delta T}{e^{\left(\frac{V_{ocn} + K_v \Delta T}{aV_t} \right)^{-1}} \quad (4)$$

wherein the terms ideal diode factor (a), nominal short-circuit current (Iscn), open circuit nominal voltage (Vocn), voltage coefficient (Kv), and thermal voltage (Vt). The combination of equations (1), (2), and (3) is used to model solar cells. The two variables that directly affect how well a solar cell functions are temperature and radiation.

B. WIND TURBINEMODEL DEVELOPMENT MODEL

Equation (5) provides an illustration of the wind turbine's aerodynamic power.

$$P_m = \frac{1}{2} \rho C_p(\beta, \lambda) A v^3_t \quad (5)$$

where Vt is the wind speed, CP is the power coefficient, λ is the speed ratio, β is the blade angle, and A is the area of the rotor blades. Pm is the mechanical power used by the wind turbine.

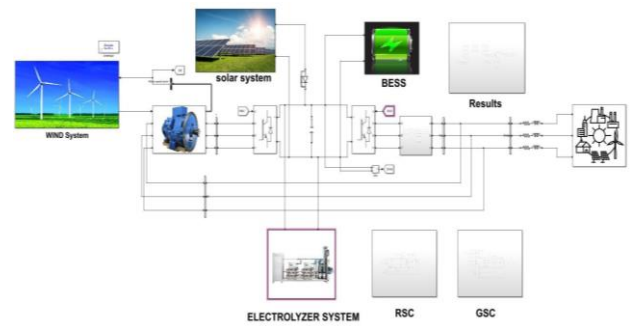


FIGURE 1. Structure of proposed grid connected hybrid system.

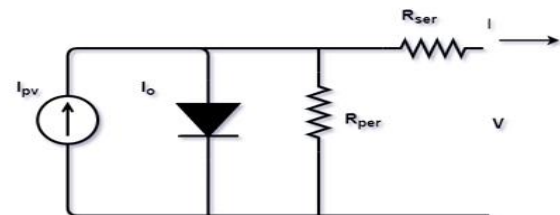


FIGURE 2. Equivalent circuit of single solar cell.

The DFIG in the suggested hybrid system is controlled by a model that is based on voltage-flux equations in the d-q reference frame [52]. The d-axis of the frame in this model is aligned with the stator's flux space vector, which continues to revolve at a synchronous speed. Equation (6) may be used to illustrate the components of the rotor current in relation to the rotor and stator equation.

$$\sigma L_r \frac{di_{dr}}{dt} = -R_r i_{dr} + \omega \sigma L_r i_{qr} + v_{dr} - \frac{L_m}{L_s} \frac{d}{dt} \phi_{ds} \quad (6)$$

$$\sigma L_r \frac{di_{qr}}{dt} = -R_r i_{qr} + \omega \sigma L_r i_{dr} + v_{qr} - \frac{L_m}{L_s} \frac{d}{dt} \phi_{qs}$$

In this case, the components for rotor current and terminal voltage are, respectively, v_{qr} , v_{dr} , i_{qr} , and i_{dr} . The rotor and synchronous speeds (rad/sec) are denoted by ω_r and ω_o . In that case, $\omega = \omega_o - \omega_r$. ϕ_{qs} and ϕ_{ds} are the components of star flux in the d-q reference. Here, R_r stands for the rotor winding resistance. The mathematical expression for the leakage component, σ , is eq. (7).

$$\sigma = \frac{L^r L^s - L^2_m}{L_s L_r} \quad (7)$$

Here, different inductance is represented by L_r , L_m , and L_s . T_e presents the machine's electromagnetic torque, which is determined by equation (8).

$$T_e = -p \frac{3L_m v_{ms}}{2L_s \omega_o} i_{qr} \quad (8)$$

The amplitude of stator voltage is denoted by v_{ms} . P_e stands for electromagnetic power, which has a mathematical expression in eq. (9).

$$P_e = -\frac{3L_m \omega_r}{2L_s \omega_o} v_{ms} i_{qr} \quad (9)$$

The formulae for rotor power (P_r) and stator power (P_s) are also provided by equation (10) using equation (9).

$$P_r = -\frac{3L_m}{2L_s} v_{ms} i_{qr}$$

$$P_s = -\frac{3L_m(\omega_o - \omega_r)}{2L_s \omega_o} \frac{L_m}{L_s} v_{ms} i_{qr}$$

1) RSCCONTROL

The RSC controls the component of terminal voltage v_{qr} and v_{dr} . Here, a sine wave pulse and modulation indices m_{qr} and m_{dr} were utilised to regulate the voltage components. The rotor current model is non-linear because of the product of the i_{qr} and i_{dr} variables. The formula "rotor current dynamics are separated" is used to determine the rotor terminal voltage.

$$\sigma L_r \frac{di_{dr}}{dt} = -R_r i_{dr} + g1$$

$$\sigma L_r \frac{di_{qr}}{dt} = -R_r i_{qr} + g2$$

Here, the two new control parameters, $g1$ and $g2$, which are dependent on m_{qr} and m_{dr} , are as follows:

$$m_{dr} = \frac{2}{V_{DC}} (g1 - \omega \sigma L_r i_{qr})$$

$$m_{qr} = \frac{2}{V_{DC}} (g2 - \omega \sigma L_r i_{dr} + \frac{L_m \omega}{L_s \omega_o} v_{ms})$$

where V_{DC} stands for DC-link voltage. (12) may be used to determine the transfer function for the I_{DR} and I_{QR} currents, such as:

$$G_{ir}(s) = \frac{I_{dr}(s)}{G_1(s)} = \frac{I_{qr}(s)}{G_2(s)} = \frac{1}{\sigma L_r s + R_r} \quad (13)$$

The basis of the zero-pole cancellation technique is the proportional integral (PI) controller, which is created in order to manage the components of the motor current. The plant transfer function's zero is represented as $SZ = -KIr$, while its pole is provided as $SP = -R_r / \sigma L_r$. Whereas Kpr indicates the proportional gain of the PI controller and Kir stands for integral gain. In order to get the proper bandwidth, the closed-loop current control

time constant T_{cr} is maintained at a value of one tenth of the switching frequency. Based on these standards, the PI controller's factors are stated as follows:

$$K_{pr} = -\frac{\sigma L_r}{T_{cr}}, \quad K_{Ir} = -\frac{R_r}{T_{cr}} \quad (14)$$

The stator's active power and circuit's active power [52] are stated as follows:

$$Q_s = \frac{3v^2 m_s L_m}{2\omega_o L_s} - \frac{3}{2} \frac{v^2 m_s L_m}{L_s} i_{dr} \quad (15)$$

$$P_s = -\frac{3L_m}{2L_s} v_{ms} i_{dr}$$

To prevent excessive motor currents and RSC loading, the IDR setpoint is often set to zero. Consequently, Fig. 3 displays the block diagram of RSC control.

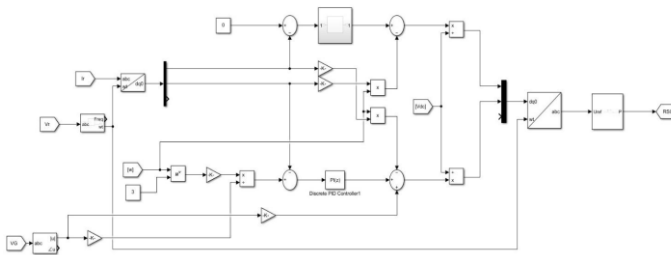


FIGURE3. Control Scheme of RSC.

2)GSC CONTROL

In the suggested model, the GSC control sensor regulates the DC-link voltage. The P&O method is also used to manage and track MPPT for PV Components of the present GSC are first being detached as follows:

$$L_g \frac{di_{dg}}{dt} = -R_g i_{dg} + L_g \omega_o i_{qg} - v_{dg} + \frac{v_{DC}}{2} m_{dg} \quad (16)$$

$$L_q \frac{di_{dq}}{dt} = -R_q i_{dq} + L_q \omega_o i_{dg} - v_{qg} + \frac{v_{DC}}{2} m_{qg}$$

where V_{dg} and V_{qg} are grid voltage components. The voltage vector of the stator in this scenario has aligned with the reference frame's x-axis, thus $V_{qs} = 0$. Upon the introduction of new variables, J_{dq} and J_{dqr} , the transfer function for the suggested system may be found as follows:

$$G_{ig}(s) = \frac{I_{dg}(s)}{J_{dg}(s)} = \frac{I_{qg}(s)}{J_{dq}(s)} = \frac{1}{L_g s + R_g} \quad (17)$$

Modulation in dices m_{qg} and m_{dg} are expressed as:

$$m_{dg} \frac{2}{V_{DC}} (J_{dg} - \omega_o L_g i_{qg} + V_{dg}) \quad (18)$$

$$m_{qg} \frac{2}{V_{DC}} (J_{qg} - \omega_o L_g i_{dg})$$

The current controller G_{cig} 's parameters are determined using a similar strategy, where K_{lig} represents the integral gain and K_{pig} represents the proportional gain.

$$K_{pig} = \frac{L_g}{T_{cig}}, \quad K_{lig} = \frac{R_g}{T_{cig}} \quad (19)$$

Closed loop transfer function GCL issued for reducing first order function, such as:

$$G_{CL} = \frac{1}{T_{cig} s + 1} \quad (20)$$

The GSC maintains the balance of electrical power between the DC and AC sides by designing a voltage control loop that connects the DC-link with the PV.

$$P_{PV} = \frac{d}{dt} \frac{1}{2} C_{DC} V_{DC}^2 + P_r + \frac{3}{2} V_{dg} i_{dg} + P_{BESS} \quad (21)$$

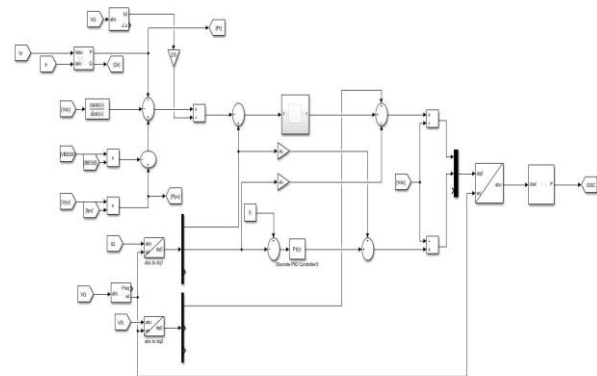


FIGURE 4. Control scheme of GSC.

When T_{cig} value is small, $i \cdot dq$ is used as control variable instead of i_{de} , and the transfer function using new variable P_c is changed.

$$G_v(S) = \frac{V_{DC}^2}{P_c} = \frac{2}{C_{DC}S} \quad (22)$$

When, $i \cdot dq$ is quite relevant to P_c , thus it can be expressed as:

$$i \times dg = \frac{2}{3V_{dg}} (-P_c + P_{pV} - P_r + P_{BESS}) \quad (23)$$

The PI controller, due to its $G_v(S)$ nature, cannot handle nonlinearities. To improve stability and remove steady state error, a lead compensator and integrator are used.

$$G_{cv}(S) = \frac{K_{lvg} s + \alpha}{s s + r} \quad (24)$$

The block diagram of GSC control, illustrating the use of lead compensator parameters α and r , is depicted in Fig. 4.

C. MODEL DEVELOPMENT OF BESS

The standard BESS model is selected and modelled as: [53], [54]:

$$V_{Bat} = E - R_b \cdot I_{Bat} \quad (25)$$

$$E = E_0 - K \cdot \frac{Q}{Q - k \cdot \int i_1 dt} + A \cdot \exp\left(-B \cdot \int i_1 dt\right) \quad (26)$$

$$SOC(\%) = 100 \left(1 - \frac{Q_d}{C_{bat}}\right) = 100 \left(1 - \frac{I_{bat} t}{C_{bat}}\right) \quad (27)$$

The supervisory control system must detect and control the BESS SoC, ensuring it maintains the required power and voltage during charge.

D. MODEL DEVELOPMENT OF FC

Renewable energy sources, such as the Solid Oxide Fuel Cell (SOFC), are gaining attention for their potential to reduce pollution and dependence on fossil fuels, making them an attractive choice for energy transition.

SOFC cells operate at high temperatures, allowing direct handling of natural gas and achieving high electric efficiencies, making them reliable for fuel-effective stationary power generation. They are suitable for stationary systems with longer working lives and can transfer excess water through steam turbines for increased electrical power generation.

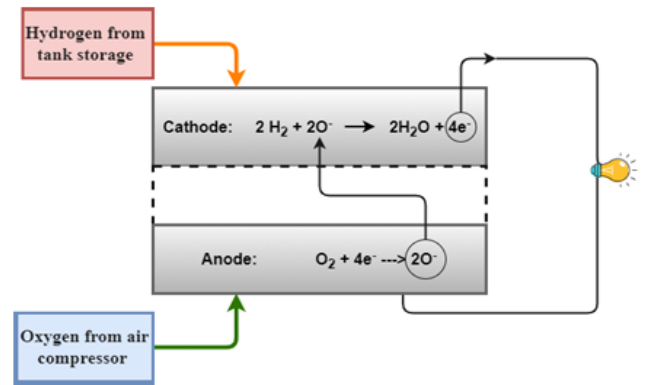


FIGURE 5. Schematic diagram of the fuel cell (SOFC type).

The SOFC consists of two electrodes, one fed with oxygen and the other with hydrogen, allowing reduction and oxidation. The electrolyte facilitates the passage of lost ions and electrons through an external circuit.

The fuel cell is a reliable and efficient technology for direct power generation and micro-grid applications, converting chemical energy into electrical energy.

The ideal voltage of open circuit cell can be determined by the Nernst expression as:

$$V_{Nernst} = -\frac{\Delta G}{2F} - \frac{RT}{2F} \ln \left(\frac{P_{H_2O} P_{ref}^{0.5}}{P_{H_2} P_{O_2}^{0.5}} \right) \quad (28)$$

The equation calculates the Gibbs free energy from a reaction in a cell, where V_{Nernst} represents the

reversible voltage, P_{ref} represents standard pressure, and G represents Gibbs free energy.

$$V_{cell} = V_{Nernst} - A_{cell} \ln \left(\frac{i_{cell}}{i_0} \right) - i_{cell} R_{inccell} - B_{cell} \ln \ln \left(1 - \frac{i_{cell}}{i_L} \right) \quad (29)$$

The text describes the equations used to determine the instantaneous change in partial pressures of water vapor and hydrogen in an anode gas flow channel.

$$\frac{dp_{H_2}^{ch}}{dt} = \frac{RT}{V_a} \left[\frac{2M_a}{P_a^{ch}} (P_{H_2}^{in} - P_{H_2}^{ch}) - \frac{i}{2F} \right] \quad (30)$$

$$\frac{dp_{H_2O}^{ch}}{dt} = \frac{RT}{V_a} \left[\frac{2M_a}{P_a^{ch}} (P_{H_2O}^{in} - P_{H_2O}^{ch}) - \frac{i}{2F} \right] \quad (31)$$

$$\frac{dp_{O_2}^{ch}}{dt} = \frac{RT}{V_a} \left[\frac{2M_a}{P_a^{ch}} (P_{O_2}^{in} - P_{O_2}^{ch}) - \frac{i}{2F} \right] \quad (32)$$

The cell voltage for a single fuel cell can be expressed mathematically as follows [57]

$$V_{CF} = n_{CF} V_{Cell} \quad (33)$$

E. MODEL DEVELOPMENT OF ELECTROLYZER

Three primary technologies, namely Solid Oxide Electrolyzer (SOE), Alkaline Electrolyzer, and Membrane Electrolyzer, can be utilized for the proton exchange electrolysis process.

Electrolyzer The working temperature range of SOE systems is quite high, ranging from 550 to 1100 °C. As a result, this high temperature improves the system's integrating potential and conversion efficiency without the need for costly catalysts. Furthermore, if extra heat sources for steam or water are reused due to high temperatures, the input energy needed for the SOE system can be reduced. The flow of current via an electrolyzer causes water to break down into hydrogen and oxygen, as demonstrated by the empirical VEC equation, which is expressed as [58] and [53]:

$$V_{Elec} = U_{rev} \frac{r_1 + r_1 T}{A_{Elec}} I_{Elec} + k \quad (34)$$

$$k = k_{Elec} \ln \left[\left(k_{T1} + \left(\frac{k_{T2}}{T} \right) + \left(\frac{k_{T3}}{T} \right) \right) \frac{I_{Elec}}{A_{Elec}} + 1 \right] \quad (35)$$

where r_1 and r_2 stand for ohmic resistances and k_{Elec} , k_{T1} , k_{T2} , and k_{T3} stand for the electrolyser's overvoltage.

Furthermore, the electrode cell's A_{Elec} represents area.

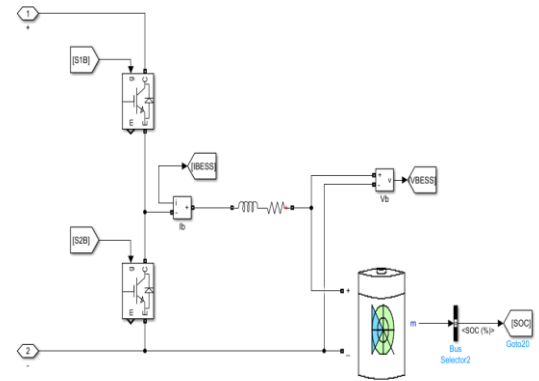


FIGURE 6. Schematic diagram of DC-DC converter associated with BESS.

IV. POWER MANAGEMENT

The purpose of any architecture for power management is to guarantee that the power is of a sufficient quality based on the type of energy that is stored. Every energy source that is being suggested has been looked into to look at the topology of power management. The charging and discharging of BESS are contingent upon the hybrid system's power usage. As a result, BESS is connected to the DC-link through a DC-DC converter that also functions as a charge controller. During the charging and discharging phases, this controller permits both positive and negative currents to flow from the BESS to the DC-link and from the DC-link to the BESS. Because the BESS's output voltage is unipolar, the battery's voltage polarity remains constant. Additionally, the DC-DC converter has both first- and second-quadrant functions [59]. Fig.6 shows the DC-DC converter for BESS, and the related equation may be found as follows:

$$L_b \frac{di_L}{dt} = V_{dc} m_b - V_b - R_b i_L \quad (36)$$

where m_b is the modulation index, V_b is the BESS voltage, and i_L is the BESS current. The battery current reference was created by dividing the ratio of P_{extra} by BESS power supply voltage. An error has been introduced into the PI controller to heterogeneously vary the duty cycles between the BESS current reference and BESS injector current.

The steps to determine the current loop reference and BESS instructions are as follows:

- P_{extra} is equivalent to the difference among the powers of the PV, GSC rating, Rotor, and FC.

$$P_{extra} = P_{PV} - P_{GSC} - P_r + P_{FC} \quad (37)$$

- P_{extra} that represents the amount of extra power is absorbed or injected by the BESS. The value of P_{extra} is favourable when solar radiation and wind speed are high BESS is meant to absorb this additional power. But when there's little sunlight or wind, velocity, this power is negative, and it shows that BESS is intended to add this negative force to the DC link.

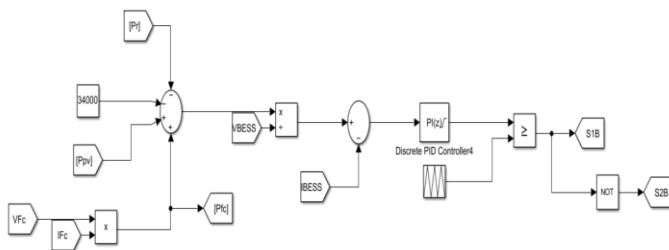


FIGURE 7. Schematic diagram of control associated with BESS

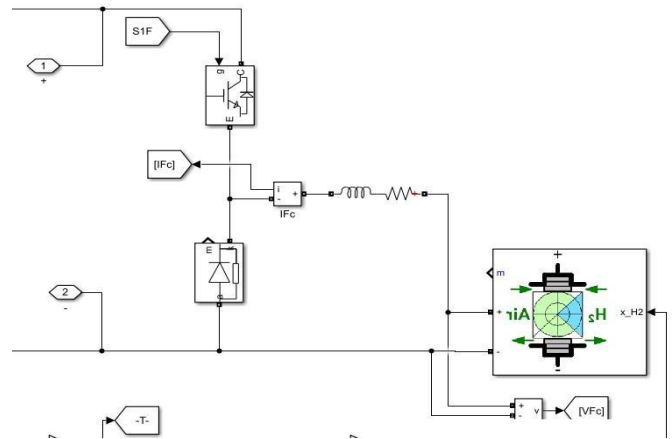


FIGURE 8. Schematic diagram of DC-DC converter controller incorporated

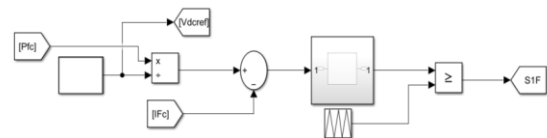


FIGURE 9. Schematic diagram of control associated with FC.

The control technique for the BESS (Battery Energy Storage System) charge controller is illustrated in Figure 7. The DC-DC Boost controller, which is linked to the duty cycle control angle and the fuel cell (FC), is depicted in Figures 8 and 9, respectively. The buck converter and electrolyzer control algorithm are shown in Figures 10 and 11.

To determine the duty cycle for the electrolyzer, the difference between the DC voltage (V_{dc}) and the electrolyser's power is used. An ANN (Artificial Neural Network) is proposed to minimize the error in the duty cycle calculation for the electrolyzer and to achieve accurate control. The ANN is trained to handle variations and nonlinearities in the system effectively. To ensure the control duty cycle value stays between 0 and 1, a limiter is added to the ANN output.

The SoC (State of Charge) range used in this work for BESS (Battery Energy Storage System)

charging and discharging is 20% to 80%. BESS can act as a source of power or a sink, depending on the conditions and the amount of electricity needed. The FC (Fuel Cell) controller and BESS are designed to handle scenarios where there is an unanticipated shift in power demand. In such scenarios, the BESS provides rapid power, and its power supply should be reduced by increasing the fuel cell's output power.

To establish the connection between the BESS and the FC, a DC boost controller and FC are proposed, aiming to achieve zero battery current. Instead of a traditional control mechanism, an ANN (Artificial Neural Network) is proposed to manage this link. The ANN will be trained to dynamically adjust the power balance between the BESS and the FC, optimizing performance and ensuring stability. The ANN's ability to learn and adapt to varying conditions will enhance the system's responsiveness and efficiency

In addition, the BESS should take the role of the FC in cases like these where the battery's SoC is only 20% in order to provide power. Therefore, the battery is being charged using the extra power generated until its shutoff. When the SoC hits its limit (80%), the leftover power is sent to the electrolyzer through a DC converter that is programmed to raise the duty cycle to enhance the voltage on the DC grid. Power goes to the electrolyzer when the battery's SoC exceeds 80% and PNET exceeds 0 to ensure proper operation. Switch provides the signal to the PI output in this instance. One way to express the produced FC power is as follows:

$$P_{FC} = P_{NET} - P_{BESS} - P_{ELEC} - P_{PV} \quad (38)$$

The suggested management and control techniques guarantee that the average power from BESS and the instantaneous electricity from the FC functions in accordance with the battery's SoC. When the SoC reaches 80% and the Electrolyzer starts to create the hydrogen that is being reserved in the tank, it should retain more energy during charging mode. On the other side, the FC need to signal a shortage of power when the SOC falls below 20% while the battery is draining. Additionally, the excess power is used to charge the BESS until it reaches the limit (80%) when there is low demand $P_{NET} > 0$ or additional wind power. The Electrolyzer then maintains the battery's functionality by holding onto its excess electricity. Even with high demand ($P_{NET} < 0$), when PV and wind power output is less, the BESS supplies the power needed by FC, ensuring the assistance progression up to the lower limit of SoC. According to the flowchart shown by Fig. 12, the associated BESS, FC, Electrolyzer, and PV are therefore responsible for ensuring the DC-grid voltage (V_{dc}) regulation.

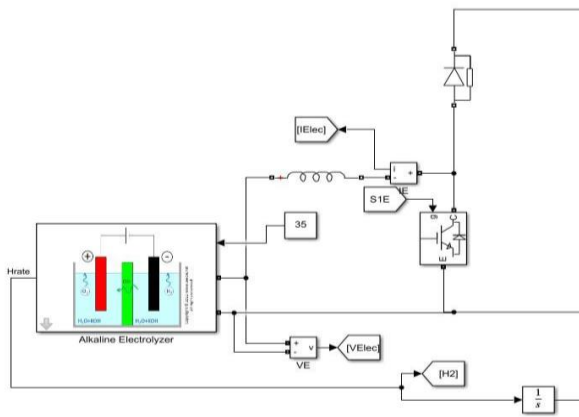


FIGURE 10. Schematic diagram of Electrolyzer with buck converter.

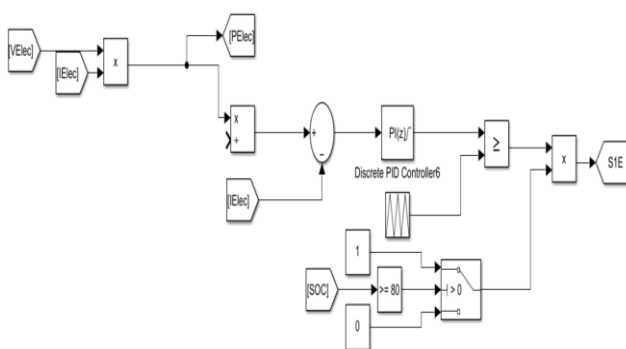


FIGURE 11. Schematic diagram of Electrolyzer control.

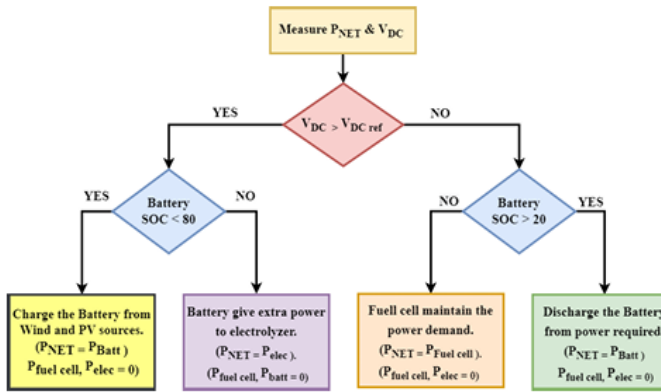


FIGURE 12. Flowchart of power management of all energy sources.

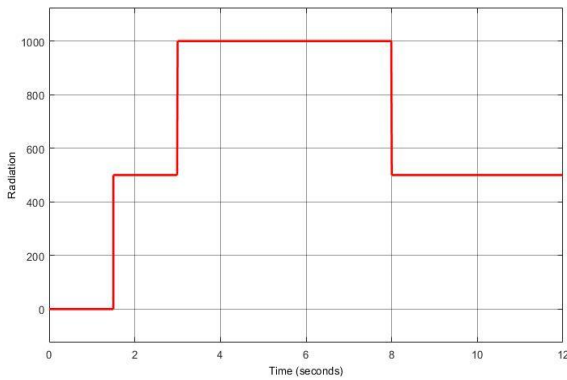


FIGURE 13. Solar irradiance ($\frac{W}{m^2}$)

V. SIMULATION AND RESULTS

This study describes the addition of the FC and Electrolyzer to the WTG-DFIG, PV, and BESS systems that are linked in a hybrid grid system. The hybrid grid-connected system has been put into practice, and MATLAB's Simulink environment is used to control electricity for the suggested system. The system as a whole was simulated with varying loads and environmental variables. This highlights how this hybrid system affects the effectiveness and calibre of the energy that is injected and/or required. To gather with the solar system, which has a capacity greater than the GSC rating, the DFIG's capacity is assumed to be 2 MW. The recommended range for GSC and RSC ratings is 24% to 31% of the generator's rating [52]. Therefore, 340 kVA and 250 kVA are assumed to be the GSC and RSC values, respectively. In contrast, 1.1 MW is assumed for the PV system rating. To accentuate the advantages of

the selected system, the system's capacity is significantly more than its GSC rating. This system is linked to a 100-Ah BESS to safeguard the GSC against overloads. The system is expanded with a 50 kW FC operating at 625 V and a 35 V electrolyzer. Table 1 lists the DFIG, WT, and GSC parameters. The results of simulating the suggested system under various conditions are given and examined in this section. As seen in Fig. 13, solar irradiance is thought to fluctuate during the course of a day. The PV system is secured by a circuit and a diode (D1). circuit breaker (SP). At $t = 0$, the circuit breaker is turned on. Until sun irradiance is 0 W/m² at $t = 2$ sec, and then it changes to 500 W/m² between $t = 2$ and 3 seconds, and 1000 W/m² between After 3 to 8 seconds, return to 500 W/m² for the remaining duration. PV electricity is reliant on solar radiation. Figure. 14 displays the PV array type current and power at MPPT. The design specifications for the PV, BESS, FC, and Electrolyzer have been provided in Table 2.

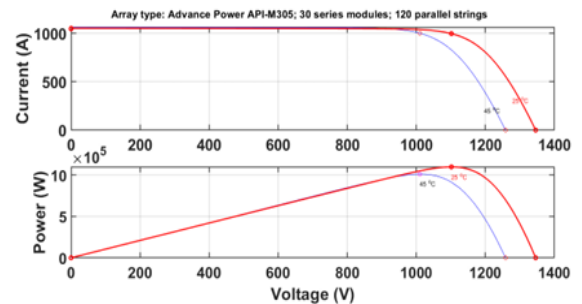


FIGURE 14. current and power at MPPT for array type (temperature variation).

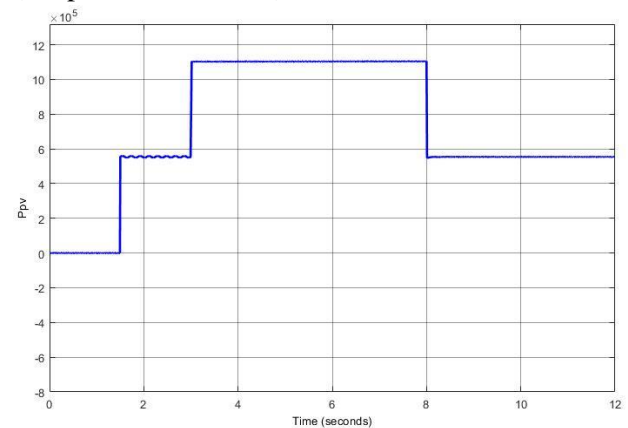


FIGURE 15. PV power (MW)

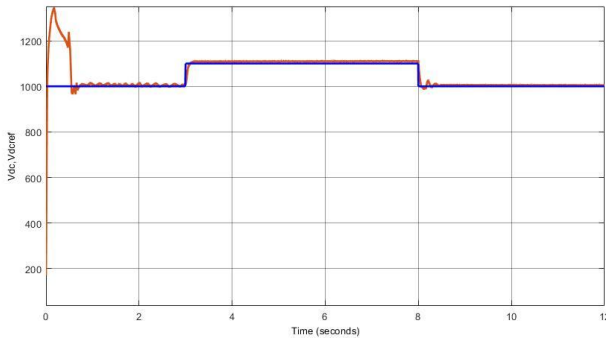


FIGURE 16. DC Bus Voltage (V).

Symbol	Parameter	Values
f	Frequency (Hz)	50
P_s	Rated Stator power (W)	2e6
n	Rated Rotational Speed (rpm)	1500
I_s	Rated Stator current (A)	1760
V_s	Rated Stator voltage (V)	690
T_{em}	Rated Torque (N.m)	12732
p	Pole pair	2
u	Stator/Rotor Turn Ratio	1/3
V_r	Rotor rated voltage (Non-Reached) (V)	2070
s_{max}	Maximum Slip	1/3
C_b	Rated Rotor voltage reference to stator	$(V_r * S_{max}) * u$
R_s	Stator leakage	$2.6e-3$
L_{si}	Leakage Inductance (stator and rotor) (H)	$0.087e-3$
L_m	Magnetization Inductance (H)	$2.5e-3$
R_r	Rotor resistance referred to stator (Ω)	$2.6e-3$
-	Stator Inductance (H)	$L_s = L_m + L_{si}$
-	Rotor Inductance (H)	$L_r = L_m + L_{si}$
V_{dc}	DC link voltage	1050 – 1150
J	Inertia	127
f_{sw}	Switching Frequency	4e3
N	Gearbox ratio	100
ρ	Air Density	1.225
β	Pitch angle	0
-	C_{pmax}	0.44
C_{bus}	DC bus capacitance	$80e-3$
R_g	Grid side filter resistance	$20e-6$
L_g	Grid side filter inductance	$400e-6$

TABLE 1. DFIG Wind turbine and GSC parameters.

PV generation reaches its maximum and is realised in 3 to 8 seconds. @ MPP, it could produce 1.1 MW of electricity at its maximum. PV is intended to inject energy into the system during this internal bus (DC).

Power from the PV and the ROTOR now flows to the GSC. It is important to make good use of this enormous power to prevent GSC overheating. Fig. 15 shows the PV

output power for the suggested arrangement. Therefore, until its SOC rises beyond 80%, BESS keeps starting to charge and absorb the additional power. After eight seconds, there is a decrease in solar irradiance, which reduces PV power output. In low solar irradiance conditions, the BESS releases stored energy to the DC connection. The DC link waveform is shown in Fig. 16. Prior to PV power generation starting up, some Although there are early transients, the DC link voltage quickly maintains because of the BESS power supply, at 1000

V. The DC link voltage reaches its reference in 3–8 seconds. level of 1158 V as a result of the PV power infusion.

It has been shown how the BESS charges and discharges when PNET is positive at the DC connection.

When the DC link does not receive excess power from PV, the BESS power is displayed in Fig. 17. It shows that the BESS is completely discharged after 8 seconds and in 1 to 2 seconds. When PV generation tracks the MPP power for three to eight seconds, negative power illustrates the charging behaviour of the BESS. BESS SoC is restricted to 20%–80%. When the SoC of the DC link is less than 80%, the BESS's function is to release power to it until it reaches 20%.

The BESS is charged during the system's first transitory behaviour. In order to sustain the power at the DC link during the second phase, the BESS began discharging for three seconds. It then charges when sufficient power from the PV side guarantees the DC link's power need.

Parameter	Values
PV parallel strings	60
Series connected modules per strings	30
Maximum power PV array (W)	213.15
Open circuit voltage V_{oc} (V)	36.3
Short circuit current I_{sc}	7.84
BESS nominal voltage (V)	800
BESS rated capacity (Ah)	100
Initial SoC BESS	50
FC Power (kW)	50
FC Voltage	625
Nominal hydrogen utilization	99.56

TABLE 2. PV, BESS, and Electrolyzer design parameters.

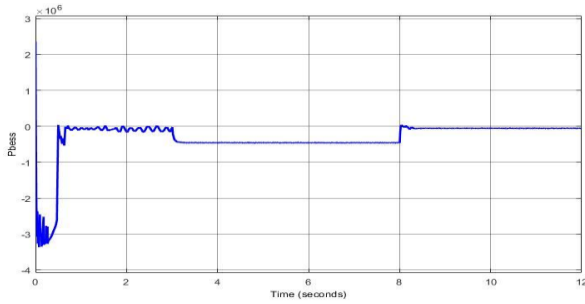


FIGURE 17. BESS discharging power (kw).

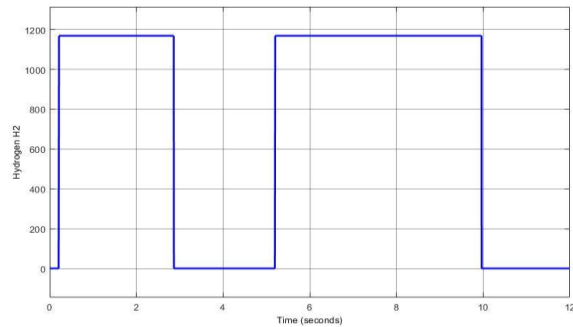


FIGURE 18. H2 production (litre).

The electrolyzer begins dissipating electricity to make and store hydrogen in the hydrogen tank when the BESS is charged to 80% and there is still extra power at the DC connection. FC connects to guarantee system stability and service continuity when BESS falls below 20%. FC then produced power for the DC link supply by using the hydrogen gas stored in the hydrogen tank. The generation and storage of H₂ in the hydrogen tank during the BESS charging phase are seen in Figs. 18 and 19.

The tank will create electricity for the DC link. Figures 18 and 19 depict H₂ production and storage in a hydrogen tank during the charging phase of BESS. Figure 20 depicts H₂ consumption.

Figures 20 and 21 show plots of the rotor powers (Active Pr) and reactive Qr. In the sub-synchronous span, positive power is extracted from the RSC, whereas in the super-synchronous span, negative power is supplied.

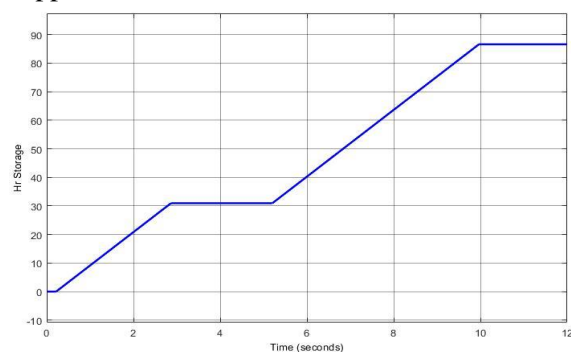


FIGURE 19. H2 storage (LITRE).

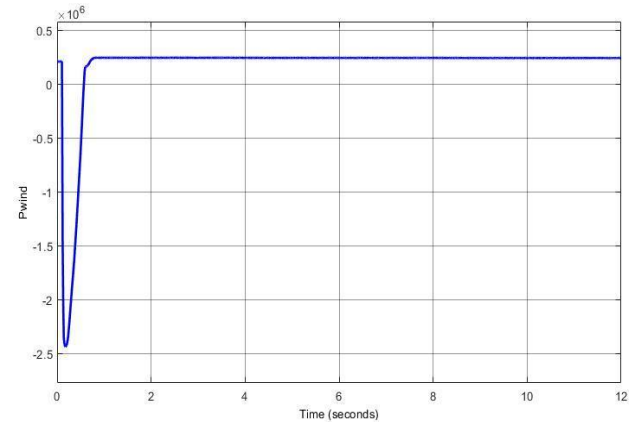


FIGURE 20. Rotor (Pr) power(W)

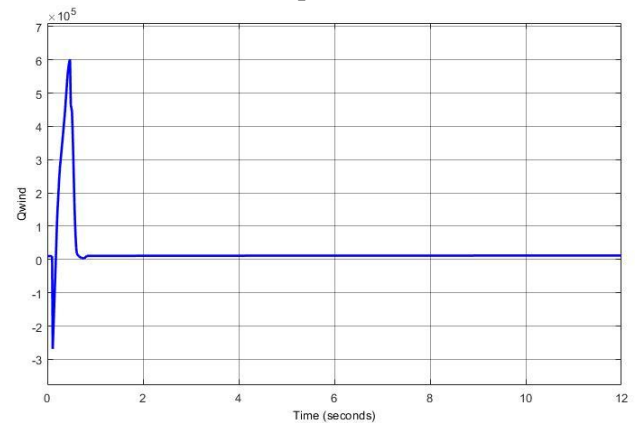


FIGURE 21. Rotor (Qr) power(W)

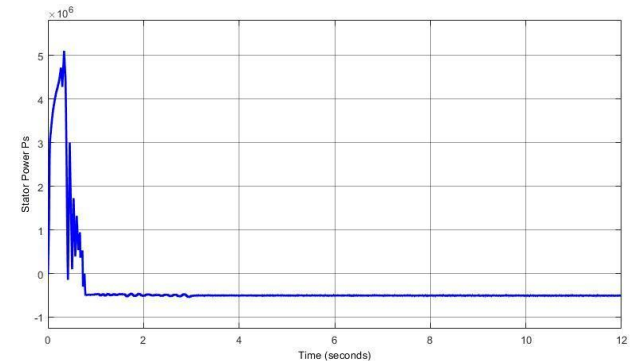


FIGURE 22. Starter (Ps) power(W)

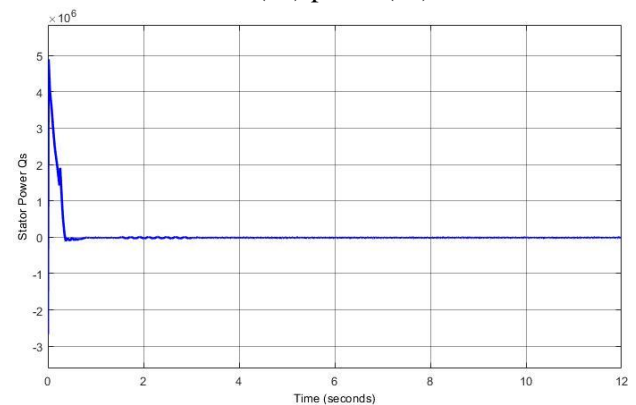


Figure 23. Stator (Qs) power(W).

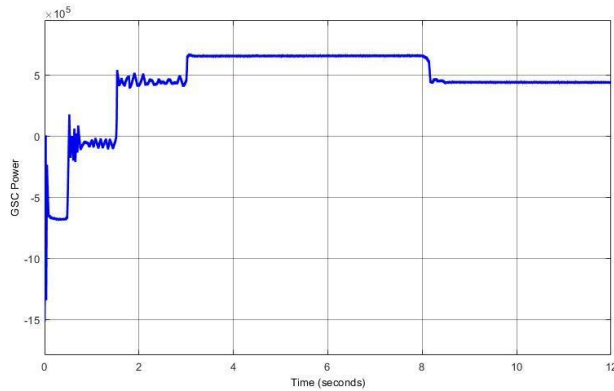


FIGURE 24. PGSC power (W).

The DC connection. Figures 22 and 23 show the stator's active and reactive powers. Active power is positive and transmitted to the grid, while reactive power is negligible (zero). Figure 24 depicts the GSC power waveform. In sub-synchronous mode, the value is lower than the rated value due to low PV irradiance or wind velocities. To maintain proper control, keep BESS and GSC values close to their rated values. Figure 25 illustrates the performance of this grid voltage. The primary purpose of the proposed the system is designed to maintain a stable voltage, hence the zoom-in feature displays the stable AC grid voltage.

Figure 26 compares the output power response of the proposed hybrid and traditional systems. The proposed architecture uses fuel cells and PV to meet energy demands and achieve the reference target.

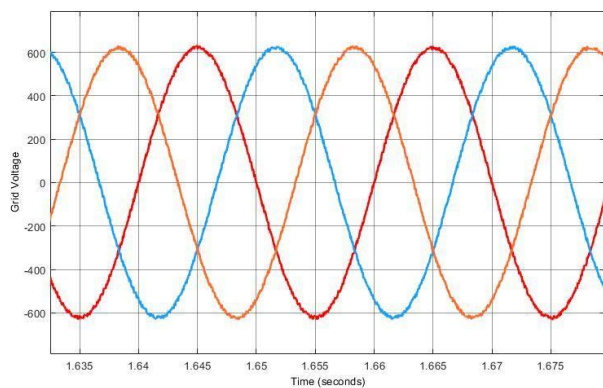


FIGURE 25. Grid Voltage (V).

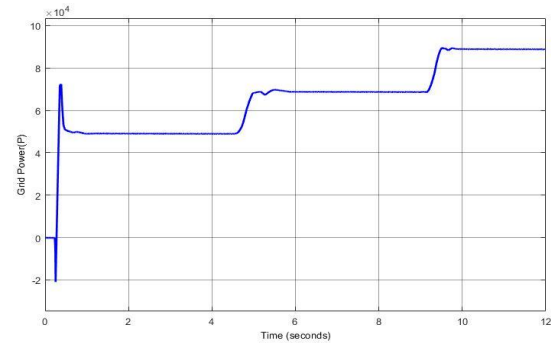


FIGURE 26. Comparative analysis of proposed hybrid and conventional power system.

VI. CONCLUSION:

This research proposes using FC and Electrolyzer as energy sources in a PV-DFIG and BESS hybrid grid-connected system with minimal converter and control loops. All system components' properties, as well as the proposed system's main configuration, are explained. This work focuses on designing controllers for grid-connected hybrid systems that use renewable distributed generators (Wind and PV) as primary sources, BESS as secondary sources, and FC with electrolyzer as tertiary. The suggested hybrid system eliminates the need for a PV converter, making it a cost-effective method for incorporating PV into hybrid systems.

The suggested system uses power management to optimize power sharing between sources. PV electricity is maximized and fed into the grid via GSC. Combining BESS, FC, and Electrolyzer reduces the impact of intermittent wind and PV power generation. Electrolyzer converts excess power from renewable distribution generating into hydrogen. FC uses hydrogen to supplement power generation under poor weather conditions. This presentation outlines power management strategies for meeting load profiles, avoiding BESS overcharging, and minimizing fluctuations from wind and PV sources.

The suggested system uses power management to optimize power sharing between sources. PV electricity is maximized and fed into the grid via GSC. Combining BESS, FC, and Electrolyzer reduces the impact of intermittent wind and PV power generation. Electrolyzer converts excess power from renewable distribution generating into hydrogen. FC uses hydrogen to supplement power generation under poor weather conditions. This presentation outlines power

management strategies for meeting load profiles, avoiding BESS overcharging, and minimizing fluctuations from wind and PV sources.

REFERENCES

- [1] J. M. Carrasco, L. G. Franquelo, J. T. Bialasiewicz, E. Galván, R. C. PortilloGuisado, M. M. Prats, J. I. León, and N. Moreno-Alfonso, “Power-electronic systems for the grid integration of renewable energy sources: A survey,” *IEEE Trans. Ind. Electron.*, vol. 53, no. 4, pp. 1002–1016, Jun. 2006.
- [2] H. HassanzadehFard, F. Tooryan, E. R. Collins, S. Jin, and B. Ramezani, “Design and optimum energy management of a hybrid renewable energy system based on efficient various hydrogen production,” *Int. J. Hydrogen Energy*, vol. 45, no. 55, pp. 30113–30128, Nov. 2020.
- [3] M. Xie, M. M. Gulzar, H. Tehreem, M. Y. Javed, and S. T. H. Rizvi, “Automatic voltage regulation of grid-connected photovoltaic system using Lyapunov based sliding mode controller: A finite—Time approach,” *Int. J. Control, Autom. Syst.*, vol. 18, no. 6, pp. 1550–1560, Jun. 2020.
- [4] F. U. Khan, M. M. Gulzar, D. Sibtain, H. M. Usman, and A. Hayat, “Variable step size fractional incremental conductance for MPPT under changing atmospheric conditions,” *Int. J. Numer. Model., Electron. Netw., Devices Fields*, vol. 33, no. 6, p. e2765, Nov. 2020.
- [5] K. A. Khan and M. Khalid, “Improving the transient response of hybrid energy storage system for voltage stability in DC microgrids using an autonomous control strategy,” *IEEE Access*, vol. 9, pp. 10460–10472, 2021.
- [6] J. Yao, H. Li, Y. Liao, and Z. Chen, “An improved control strategy of limiting the DC-link voltage fluctuation for a doubly fed induction wind generator,” *IEEE Trans. Power Electron.*, vol. 23, no. 3, pp. 1205–1213, May 2008.
- [7] B. Benlahbib, N. Bouarroudj, S. Mekhilef, D. Abdeldjalil, T. Abdelkrim, F. Bouchafaa, and A. Lakhdari, “Experimental investigation of power management and control of a PV/wind/fuel cell/battery hybrid energy system microgrid,” *Int. J. Hydrogen Energy*, vol. 45, no. 53, pp. 29110–29122, Oct. 2020. 23257 VOLUME 11, 2023 M. M. Gulzar et al.: Innovative Converterless Solar PV Control Strategy
- [8] A. Khan, H. Ahmad, S. M. Ahsan, M. M. Gulzar, and S. Murawwat, “Coordinated LVRT support for a PMSG-based wind energy conversion system integrated into a weak AC-grid,” *Energies*, vol. 14, no. 20, p. 6588, Oct. 2021.
- [9] J. P. Da Costa, H. Pinheiro, T. Degner, and G. Arnold, “Robust controller for DFIGs of grid-connected wind turbines,” *IEEE Trans. Ind. Electron.*, vol. 58, no. 9, pp. 4023–4038, Sep. 2011.
- [10] C. Liu, F. Blaabjerg, W. Chen, and D. Xu, “Stator current harmonic control with resonant controller for doubly fed induction generator,” *IEEE Trans. Power Electron.*, vol. 27, no. 7, pp. 3207–3220, Jul. 2011.
- [11] H. Xu, J. Hu, and Y. He, “Operation of wind-turbine-driven DFIG systems under distorted grid voltage conditions: Analysis and experimental validations,” *IEEE Trans. Power Electron.*, vol. 27, no. 5, pp. 2354–2366, May 2012.
- [12] H. Nian and Y. Song, “Direct power control of doubly fed induction generator under distorted grid voltage,” *IEEE Trans. Power Electron.*, vol. 29, no. 2, pp. 894–905, Feb. 2014.
- [13] M. M. Gulzar, D. Sibtain, A. F. Murtaza, S. Murawwat, M. Saadi, and A. Jameel, “Adaptive fuzzy based optimized proportional-integral controller to mitigate the frequency oscillation of multi-area photovoltaic thermal system,” *Int. Trans. Electr. Energy Syst.*, vol. 31, no. 1, 2021, Art. no. e12643.
- [14] Z. Dejia, Z. Zhengming, M. Eltawil, and Y. Liqiang, “Design and control of a three-phase grid-connected photovoltaic system with developed maximum power point tracking,” in *Proc. 23rd Annu. IEEE Appl. Power Electron. Conf. Expo.*, Feb. 2008, pp. 973–979.
- [15] M. Gulzar, S. Rizvi, M. Javed, D. Sibtain, and R. S. Ud Din, “Mitigating the load frequency fluctuations of interconnected power systems using model predictive controller,” *Electronics*, vol. 8, no. 2, p. 156, Feb. 2019.
- [16] M. Maaruf, K. Khan, and M. Khalid, “Robust control for optimized islanded and grid-connected operation of solar/wind/battery hybrid energy,” *Sustainability*, vol. 14, no. 9, p. 5673, May 2022.

- [17] M. Hanan, X. Ai, M. Y. Javed, M. Majid Gulzar, and S. Ahmad, "A two stage algorithm to harvest maximum power from photovoltaic system," in Proc. 2ndIEEEConf.EnergyInternetEnergySyst.Integr.(EI2), Oct. 2018, pp. 1–6.
- [18] H. Ghoddami, M. B. Delghavi, and A. Yazdani, "An integrated wind photovoltaic-battery system with reduced power-electronic interface and fast control for grid-tied and off-grid applications," *Renew. Energy*, vol. 45, pp. 128–137, Sep. 2012.
- [19] R. G. Wandhare and V. Agarwal, "Novel integration of a PV-wind energy system with enhanced efficiency," *IEEE Trans. Power Electron.*, vol. 30, no. 7, pp. 3638–3649, Jul. 2015.
- [20] M.Y.Javed, M.M.Gulzar, S.T.H.Rizvi, and A.Arif, "A hybrid technique to harvest maximum power from PV systems under partial shading conditions," in Proc. Int. Conf. Emerg. Technol. (ICET), Oct. 2016, pp. 1–5.
- [21] S.Diaf, G.Notton, M.Belhamel, M.Haddadi, and A.Louche, "Design and techno-economical optimization for hybrid PV/wind system under various meteorological conditions," *Appl. Energy*, vol. 85, no. 10, pp. 968–987, Oct. 2008.
- [22] B.N.Alhasnawi, B. H.Jasim, Z.-A.-S. A. Rahman, and P. Siano, "A novel robust smart energy management and demand reduction for smart homes based on internet of energy," *Sensors*, vol. 21, no. 14, p. 4756, Jul. 2021.
- [23] S. Dorahaki, R. Dashti, and H. R. Shaker, "Optimal energy management in the smart microgrid considering the electrical energy storage system and the demand-side energy efficiency program," *J. Energy Storage*, vol. 28, Apr. 2020, Art. no. 101229.
- [24] T.M.Gür, "Review of electrical energy storage technologies, materials and systems: Challenges and prospects for large-scale grid storage," *Energy Environ. Sci.*, vol. 11, no. 10, pp. 2696–2767, 2018.
- [25] Y.Alhumaid, K.Khan, F.Alismail, and M. Khalid, "Multi-input nonlinear programming based deterministic optimization framework for evaluating microgrids with optimal renewable-storage energy mix," *Sustainability*, vol. 13, no. 11, p. 5878, May 2021.
- [26] M. Khalid, "A review on the selected applications of battery supercapacitor hybrid energy storage systems for microgrids," *Energies*, vol. 12, no. 23, p. 4559, Nov. 2019.
- [27] H. T. Dinh, J. Yun, D. M. Kim, K. Lee, and D. Kim, "A home energy management system with renewable energy and energy storage utilizing main grid and electricity selling," *IEEE Access*, vol. 8, pp. 49436–49450, 2020. 23258
- [28] A.Khatamianfar, M.Khalid, A.V.Savkin, and V.G.Agelidis, "Improving wind farm dispatch in the Australian electricity market with battery energy storage using model predictive control," *IEEE Trans. Sustain. Energy*, vol. 4, no. 3, pp. 745–755, Jul. 2013.
- [29] D. Sibtain, A. F. Murtaza, N. Ahmed, H. A. Sher, and M. M. Gulzar, "Multi control adaptive fractional order PID control approach for PV/wind connected grid system," *Int. Trans. Electr. Energy Syst.*, vol. 31, no. 4, 2021, Art. no. e12809.
- [30] C. Ghenai, M. Bettayeb, B. Brdjanin, and A. K. Hamid, "Hybrid solar PV/PEM fuel cell/diesel generator power system for cruise ship: A case study in Stockholm, Sweden," *Case Stud. Thermal Eng.*, vol. 14, Sep. 2019, Art. no. 100497.
- [31] M. Çolak and İ. Kaya, "Multi-criteria evaluation of energy storage technologies based on hesitant fuzzy information: A case study for Turkey," *J. Energy Storage*, vol. 28, Apr. 2020, Art. no. 101211.
- [32] L. Kong, J. Yu, and G. Cai, "Modeling, control and simulation of a photovoltaic /hydrogen /supercapacitor hybrid power generation system for grid-connected applications," *Int. J. Hydrogen Energy*, vol. 44, no. 46, pp. 25129–25144, Sep. 2019.
- [33] R. Amirante, E. Cassone, E. Distaso, and P. Tamburrano, "Overview on recent developments in energy storage: Mechanical, electrochemical and hydrogen technologies," *Energy Convers. Manage.*, vol. 132, pp. 372–387, Jan. 2017.
- [34] U.Akram and M.Khalid, "A coordinated frequency regulation framework based on hybrid battery-ultracapacitor energy storage technologies," *IEEE Access*, vol. 6, pp. 7310–7320, 2017.
- [35] Z. Wang, Y. Jia, C. Cai, Y. Chen, N. Li, M. Yang, and Q. Li, "Study on the optimal configuration of a wind-solar-battery-fuel cell system based on a

- regional power supply,” *IEEE Access*, vol. 9, pp. 47056–47068, 2021.
- [36] K.A.Khan and M.Khalid, “Hybrid energy storage system for voltage stability in a DC microgrid using a modified control strategy,” in *Proc. IEEE Innov. Smart Grid Technol. Asia (ISGT Asia)*, May 2019, pp. 2760–2765.
- [37] T.Ma, H.Yang, and L.Lu, “Development of hybrid battery–supercapacitor energy storage for remote area renewable energy systems,” *Appl. Energy*, vol. 153, pp. 56–62, Sep. 2015.
- [38] M. M. Gulzar, M. Iqbal, S. Shahzad, H. A. Muqet, M. Shahzad, and M. M. Hussain, “Load frequency control (LFC) strategies in renewable energy-based hybrid power systems: A review,” *Energies*, vol. 15, no. 10, p. 3488, May 2022.
- [39] L. Zhang, X. Hu, Z. Wang, F. Sun, and D. G. Dorrell, “A review of super capacitor modeling, estimation, and applications: A control/management perspective,” *Renew. Sustain. Energy Rev.*, vol. 81, no. 2, pp. 1868–1878, 2018.
- [40] F. Nejabatkhah, S. Danyali, S. H. Hosseini, M. Sabahi, and S. M. Niapour, “Modeling and control of a new three-input DC–DC boost converter for hybrid PV/FC/battery power system,” *IEEE Trans. Power Electron.*, vol. 27, no. 5, pp. 2309–2324, May 2012.
- [41] Y.-M. Chen, C.-S. Cheng, and H.-C. Wu, “Grid-connected hybrid PV/wind power generation system with improved DC bus voltage regulation strategy,” in *Proc. 21st Annu. IEEE Appl. Power Electron. Conf. Expo.*, Mar. 2006, p. 7.
- [42] X. Li, D. Hui, and X. Lai, “Battery energy storage station (BESS)-based smoothing control of photovoltaic (PV) and wind power generation fluctuations,” *IEEE Trans. Sustain. Energy*, vol. 4, no. 2, pp. 464–473, Apr. 2013.
- [43] S. S. Martin, A. Chebak, A. El Ouafi, and M. Mabrouki, “Modeling and simulation of hybrid power system integrating wind, solar, biodiesel energies and storage battery,” in *Proc. Int. Renew. Sustain. Energy Conf. (IRSEC)*, Nov. 2016, pp. 457–463.
- [44] R. Sebastián, “Battery energy storage for increasing stability and reliability of an isolated wind diesel power system,” *IET Renew. Power Gener.*, vol. 11, no. 2, pp. 296–303, Feb. 2017.
- [45] B. P. Hayes, A. Wilson, R. Webster, and S. Z. Djokic, “Comparison of two energy storage options for optimum balancing of wind farm power outputs,” *IET Gener., Transmiss. Distrib.*, vol. 10, no. 3, pp. 832–839, 2016.
- [46] L. Qu and W. Qiao, “Constant power control of DFIG wind turbines with supercapacitor energy storage,” *IEEE Trans. Ind. Appl.*, vol. 47, no. 1, pp. 359–367, Jan. 2011.
- [47] G. Lei, H. Song, and D. Rodriguez, “Power generation cost minimization of the grid-connected hybrid renewable energy system through optimal sizing using the modified seagull optimization technique,” *Energy Rep.*, vol. 6, pp. 3365–3376, Nov. 2020. VOLUME 11, 2023 M. M. Gulzar et al.: Innovative Converterless Solar PV Control Strategy
- [48] M. B. Camara, B. Dakyo, and H. Gualous, “Polynomial control method of DC/DC converters for DC-bus voltage and currents management—Battery and supercapacitors,” *IEEE Trans. Power Electron.*, vol. 27, no. 3, pp. 1455–1467, Mar. 2012.
- [49] S. Adhikari and F. Li, “Coordinated V-f and P-Q control of solar photovoltaic generators with MPPT and battery storage in microgrids,” *IEEE Trans. Smart Grid*, vol. 5, no. 3, pp. 1270–1281, May 2014.
- [50] S. Najafi-Shad, S. M. Barakati, and A. Yazdani, “An effective hybrid wind photovoltaic system including battery energy storage with reducing control loops and omitting PV converter,” *J. Energy Storage*, vol. 27, Feb. 2020, Art. no. 101088.
- [51] M. G. Villalva, J. R. Gazoli, and E. R. Filho, “Comprehensive approach to modeling and simulation of photovoltaic arrays,” *IEEE Trans. Power Electron.*, vol. 24, no. 5, pp. 1198–1208, May 2009.
- [52] G. Abad, J. Lopez, M. Rodriguez, L. Marroyo, and G. Iwanski, *Doubly Fed Induction Machine: Modeling and Control for Wind Energy Generation*. Hoboken, NJ, USA: Wiley, 2011.
- [53] Y. Xu and X. Shen, “Optimal control based energy management of multiple energy storage systems in a microgrid,” *IEEE Access*, vol. 6, pp. 32925–32934, 2018.

- [54] M. Aly, E. M. Ahmed, H. Rezk, and E. A. Mohamed, "Marine predators algorithm optimized reduced sensor fuzzy-logic based maximum power point tracking of fuel cell-battery standalone applications," *IEEE Access*, vol. 9, pp. 27987–28000, 2021.
- [55] M.S.Guney and Y.Tepe, "Classification and assessment of energy storage systems," *Renew.Sustain.Energy Rev.*, vol.75, pp. 1187–1197, Aug.2017.
- [56] S. Buchaniec, A. Sciazko, M. Mozdierz, and G. Brus, "A novel approach to the optimization of a solid oxide fuel cell anode using evolutionary algorithms," *IEEE Access*, vol. 7, pp. 34361–34372, 2019.
- [57] N. Benyahia, H. Denoun, M. Zaouia, T. Rekioua, and N. Benamrouche, "Power system simulation of fuel cell and supercapacitor based electric vehicle using an interleaving technique," *Int. J. Hydrogen Energy*, vol. 40, no. 45, pp. 15806–15814, Dec. 2015.
- [58] M. Ceraolo, G. Lutzemberger, and D. Poli, "State-of-charge evaluation of supercapacitors," *J. Energy Storage*, vol. 11, pp. 211–218, Jun. 2017.
- [59] A. M. Trzynadlowski, *Introduction to Modern Power Electronics*. Hoboken, NJ, USA: Wiley, 2015.